Coherent Rayleigh–Brillouin scattering measurements of bulk viscosity of polar and nonpolar gases, and kinetic theory

A. S. Meijer,[1] A. S. de Wijn,[1] M. F. E. Peters,[1] N. J. Dam,[1] and W. van de Water[2,a)]

[1]*Institute for Molecules and Materials, Radboud University Nijmegen, Heyendaalseweg 135, NL-6525 AJ Nijmegen, The Netherlands*
[2]*Department of Physics, Eindhoven University of Technology, P.O. Box 513, 5600 MB Eindhoven, The Netherlands*

We investigate coherent Rayleigh–Brillouin spectroscopy as an efficient process to measure the bulk viscosity of gases at gigahertz frequencies. Scattered spectral distributions are measured using a Fizeau spectrometer. We discuss the statistical error due to the fluctuating mode structure of the used pump laser. Experiments were done for both polar and nonpolar gases and the bulk viscosity was obtained from the spectra using the Tenti S6 model. Results are compared to simple classical kinetic models of molecules with internal degrees of freedom. At the extremely high (gigahertz) frequencies of our experiment, most internal vibrational modes remain frozen and the bulk viscosity is dominated by the rotational degrees of freedom. Our measurements show that the molecular dipole moments have unexpectedly little influence on the bulk viscosity at room temperature and moderate pressure. © *2010 American Institute of Physics*. [doi:10.1063/1.3491513]

I. INTRODUCTION

In studies of nonresonant light scattering processes in gases, the methods of kinetic theory are very successful in predicting the power spectra measured in experiments, producing results of practical interest. For example, the European Space Agency (ESA) Earth Explorer Atmospheric Dynamics Mission will provide global observations of wind profiles from space utilizing the active Doppler wind lidars method.[1] The absolute frequency shift of a narrow laser line scattered off atmospheric gas molecules will be used to determine the wind speed, while the spectral distribution of the scattered light can provide other macroscopic information, such as temperature and pressure.

Line shapes in spontaneous Rayleigh–Brillouin scattering (SRBS) have been predicted most succesfully[2–4] by the theoretical model developed by Boley *et al.*[5] and Tenti *et al.*[6] In this model, information regarding the Boltzmann collision integral is obtained from transport coefficients. Pan *et al.* successfully extended the model of Boley *et al.*[5] to predict coherent Rayleigh–Brillouin scattering (CRBS) and reported good agreement with experimental data on several monatomic and molecular gases.[7–9] The transport coefficients used in the Tenti model are the shear viscosity η, the heat conductivity σ, the heat capacity c_{int}, and the bulk viscosity η_b. The latter is the most controversial parameter and at the same time has considerable influence on the line shape.[9]

Recently, it was suggested by Xu *et al.* and Pan *et al.*[9–11] that CRBS experiments can be used as an alternative method to measure bulk viscosity. The advantage is the superior signal to noise ratio of coherent Rayleigh–Brillouin scattering experiments. In this work, we use the Tenti S6 model and the well-documented values of the other transport coefficients to determine the bulk viscosity from the coherent Rayleigh–Brillouin scattering spectrum in a least-squares fitting procedure.

The bulk (or volume) viscosity η_b quantifies the resistance of a gas to rapid compression. The bulk viscosity contributes to the absorption and dispersion of sound waves in gases and is an important parameter in nonequilibrium gas dynamics, such as supersonic flows. It can be directly related to the finite relaxation time of the internal degrees of freedom, which is proportional to the mean time between collisions. In monatomic gases at room temperature, the internal electronic modes and the motion of the center-of-mass decouple, and so the bulk viscosity is equal to zero. However, in molecular gases, rotational and vibrational modes may couple to the momentum.[12,13] In spite of this, in molecular gas simulations the bulk viscosity is often set to zero because the bulk viscosity for many gases is not well-known and because the systems in question are often not compressed rapidly. In high-frequency sound waves, such as those in SRBS and CRBS experiments, however, compression and expansion are much more rapid and the dampening due to the bulk viscosity becomes important.

Rayleigh–Brillouin scattering is caused by scattering of light with a wavelength comparable to the wavelength of sound waves. The sound waves in our experiment, therefore, have frequencies of a few gigahertz, which are only one order of magnitude larger than collision frequencies at 1 bar. What previous measurements of the bulk viscosity exist have been based on sound wave attenuation in the frequency range of several megahertz and have been done only for a limited number of gases. However, because some internal degrees of freedom associated with vibrational modes may couple very weakly, they only become detectable at long time scales or only become accessible at high temperatures. The relaxation time thus depends on temperature and the bulk viscosity gen-

---
a)Electronic mail: w.v.d.water@tue.nl.

erally depends on the frequency and temperature. The bulk viscosity at the gigahertz frequencies of light scattering experiments must therefore be considered terra incognita.

In this paper, we discuss a few simple models that can express these and other intuitive connections between the bulk viscosity and molecular structure. In these models, molecules are described as rigid, classical objects which can exchange rotational energy. As the rotational quantum states are close together compared to the available energy at room temperature, a classical description is valid for describing the dynamics of rotation, and therefore the bulk viscosity.

As the bulk viscosity is the transport coefficient which is most strongly affected by internal degrees of freedom, a comparison between simple, classical, kinetic models and experimental results provides insight into the relation between the internal molecular structure and transport coefficients. It should be noted, however, that such simple models cannot be expected to reproduce the measured bulk viscosities with high accuracy. Such insight is essential for developing successful methods for predicting other transport properties such as the shear viscosity of mixtures along the lines of Refs. 14 and 15, for which shape-related effects are essential (see, for instance, Ref. 16). Polar molecules are particularly interesting in this context, as many large molecules have dipole moments, and it is expected that the dipole moment leads to a strong interaction between translational and rotational degrees of freedom, thus giving rise to a low bulk viscosity.

In Sec. II, we discuss the experiment, the least-squares procedure, and the uncertainty in the measured η_b and we present results for the nonpolar gases N_2, O_2, CO_2, CH_4, C_2H_4, and C_2H_6, and the polar gases SO_2 and H_2S. The kinetic models are described in Sec. III and compared to the experimental results. In Sec. IV, we discuss the importance of vibrational degrees of freedom and the relevance of molecular dipole moments for η_b. Conclusions are drawn and further directions of research, including a way to improve the experimental technique, are discussed in Sec. V.

II. EXPERIMENT

In coherent Rayleigh–Brillouin scattering experiments, density perturbations (sound waves) are induced by dipole forces in the electric field of two counterpropagating broad-band laser beams. Light from a second, narrow-band probe laser is scattered coherently off these density waves and the scattered light again propagates as a laser beam. Compared to spontaneous Rayleigh–Brillouin scattering, where the scattered light is distributed over more or less a 4π solid angle, this leads to a dramatic enhancement of the scattered light intensity and, as we argue here, Rayleigh–Brillouin spectra could, in principle, be collected in a single shot of a pulsed laser which lasts a mere 7 ns. In our experiments, however, the statistical error due to the fluctuating mode structure of the used pump laser necessitates averaging over laser shots.

The experimental setup follows the two-dimensional backward scattering configuration of Pan *et al.*[8] and that of
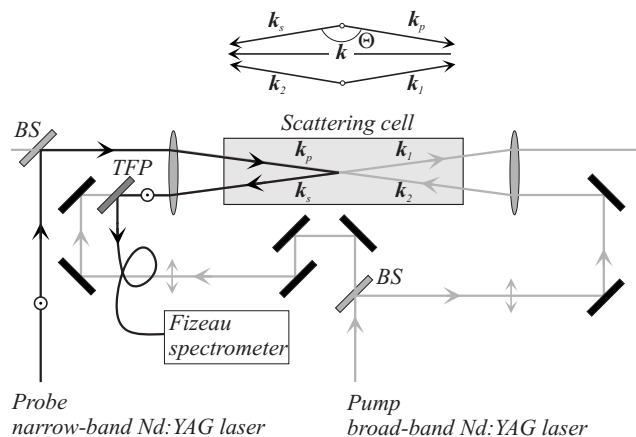

FIG. 1. Schematic diagram of the experimental setup (not to scale). The counterpropagating pump beams with wave vectors k_1, k_2 are indicated in gray; the probe laser beam with wave vector k_p and the scattered light beam with k_s are black. The scattered light is collected in a single-mode optical fiber and transported to the Fizeau spectrometer. A thin-film polarizer is indicated by TFP; beam splitters by BS. The polarization directions are indicated by $\updownarrow$, $\odot$. The arrangement of the wave vectors corresponding to the phase-matching condition is indicated.

Grinstead and Barker,[17] who first described the physical interpretation of the spectra obtained. A diagram of the setup is shown in Fig. 1. Two broad-band pump laser beams with wave vectors k_1 and k_2 are focused with 500 mm focal-length lenses and cross at their foci under an angle of 178°. The counterpropagating beams form multiple optical gratings in which gas molecules are polarized and subjected to a force toward the high electric field regions. This dipole force creates moving periodic density perturbations in the gas with angular frequency $\omega = \omega_1 - \omega_2$ and propagation vector $k = k_2 - k_1$ perpendicular to the fringes. Due to the wide bandwidth of the pump laser, the generated density perturbations also have a wide spectral distribution. The density waves are probed by Bragg diffraction of a narrow-band laser with wave vector k_p off the induced density gratings. Optical coherence requires phase matching with, in our experiment, the consequence that the signal beam k_s propagates in opposite direction to the pump beam k_1, $k_2 - k_1 = k = k_s - k_p$. The signal beam maintains the probe beam's characteristics, such as its polarization, but it will be spectrally broadened due to the interaction with the broad superposition of acoustical waves with frequency $\omega_s - \omega_p = \omega = \omega_1 - \omega_2$.

The gas to be investigated is inside a stainless steel cell of 0.5 m length equipped with optical windows. The cell allows for control of the gas conditions, such as composition and pressure. The pump laser is a Q-switched, frequency-doubled, broad-band, Nd:YAG laser with 10 ns pulse duration (manufactured by Quantel). The laser bandwidth is estimated to be 24 GHz full width half maximum (FWHM) with a 250 MHz mode structure. The narrow-band probe laser is an injection-seeded, frequency-doubled, pulsed Nd:YAG laser with a FWHM of 150 MHz and 7 ns pulse duration (manufactured by SpectraPhysics). Typical pulse energies are 8 and 2 mJ for the pump and probe beams, respectively. As the peak power densities remain much smaller than 10^{15} W m^{-2}, our experiment is in the perturbative regime.[18–20]
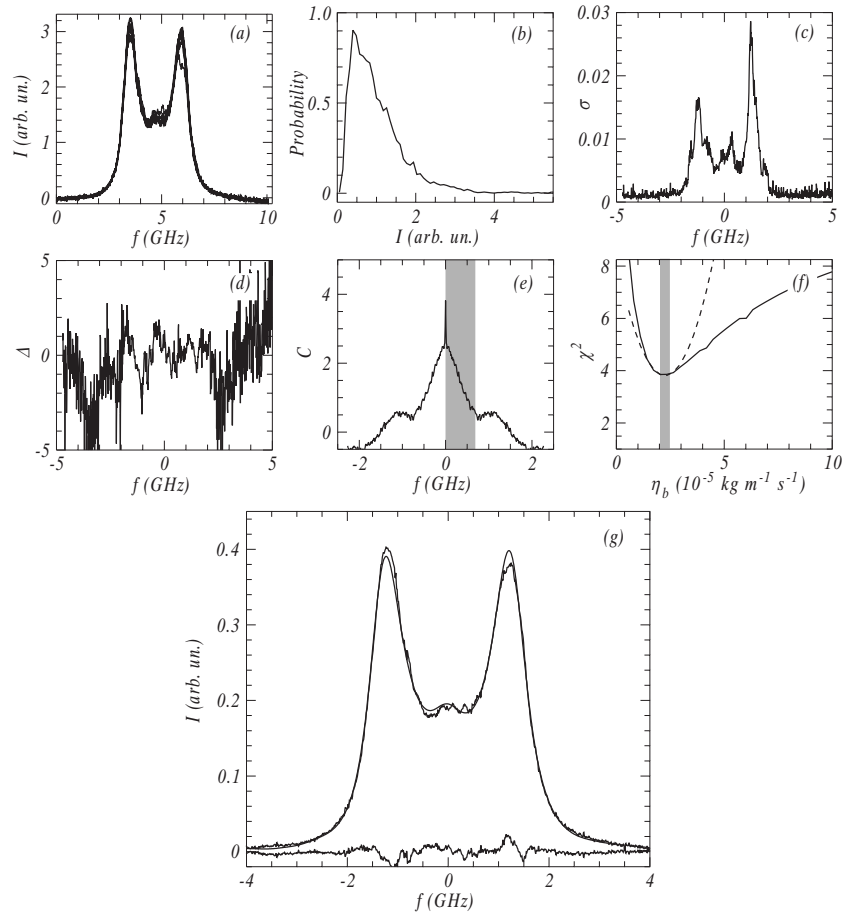
FIG. 2. Analyzing coherent Rayleigh–Brillouin scattering spectra in O_2 at $p=5$ bar ($y=2.6$). (a) Superposition of ten spectra, each averaged over 500 laser shots. The origin of the frequency scale is arbitrary; only after averaging is the center of the spectra placed at $f=0$. (b) Probability density function of pump laser intensity fluctuations in a frequency interval of 180 MHz around the central frequency. The mean intensity is normalized to 1. (c) Root-mean-square fluctuation $\sigma(f)$ of registered spectra estimated from the spectra in (a). The scale is the same as that of the mean spectrum in (g). (d) Normalized difference [Eq. (2)] between model and measured spectrum. (e) Correlation function of normalized difference between model and measurement, showing that the error consists of white noise (the narrow spike) and pump laser fluctuations, the correlation length of which is indicated by the gray band. (f) Full line: χ^2 as a function of η_b, showing minimum at $\eta_b=2.3\times10^{-5}$ kg m^{-1} s^{-1}; dashed line: fit of quadratic function to find $d^2\chi^2/d\eta_b^2$ in the minimum. This leads to the estimated statistical error $\sigma_{\eta_b}=0.3\times10^{-5}$ kg m^{-1} s^{-1}. The estimated η_b is indicated by the gray band with width σ_{η_b}. (g) Comparison of averaged spectrum to Tenti S6 model at $\eta_b=2.3\times10^{-5}$ kg m^{-1} s^{-1}.

The probe beam is polarized perpendicularly with respect to the polarization of the pump beams and the signal beam is separated from the pump beam path using a thin-film polarizer. This arrangement avoids possible interferences between pump and probe beams, and its associated complexities.

A customized fiber-coupled Fizeau spectrometer (Angstrom Co Ltd., HighFinesse GmbH) is used to measure the scattered frequency distribution. The Fizeau spectrometer is based on the same fundamental principles of multiple beam interference as a Fabry–Pérot etalon.[21] The advantage of this device is that all frequencies are measured simultaneously. The spectrum is directly imaged onto a charge-coupled device (CCD) array, with a simple relation between frequency and position. As the mirrors in the Fizeau spectrometer are not parallel, the spectral response to monochromatic light is slightly asymmetric.[22–24] This was measured in a separate experiment and the result was used to convolve the Rayleigh–Brillouin scattering spectra computed from the Tenti model. The distance between the mirrors determines the free spectral range (FSR), the mirror reflectivity determines the finesse, and the wedge angle the spectral dispersion. The FSR is mapped onto 1135 pixels (pixel size 14 μm) of the CCD array. Our Fizeau spectrometer has a FSR of 10.06 GHz, a finesse of 56, and a resolution of 250 MHz.

The presence of the longitudinal mode structure of the pump laser, which randomly fluctuates between successive pulses, is the largest source of noise in the registered coherent Rayleigh–Brillouin spectra and necessitates averaging of the spectrum over multiple laser shots. A histogram of the intensity in a narrow frequency band is shown in Fig. 2(b), demonstrating a large variation of the shot to shot laser intensity. Our spectra are the average over ten independent spectra, each of which is an average over 500 laser shots. Consequently, each spectrum is acquired in approximately 8 min, which is much faster than in experiments that use a frequency-scanning laser or a scanning spectrometer. Long time averages would show the periodic mode structure of the pump laser multiplied with the spectrum. However, since the resolution of the spectrometer equals the mode spacing of the

pump laser, the mode structure is barely visible in the Rayleigh–Brillouin spectra and it was not necessary to remove it by filtering, as was done in Ref. 8.

In principle, accurate single-shot coherent Rayleigh–Brillouin spectra can be obtained using a pump laser with a smooth and reproducible broad-band spectrum. In this way, the instantaneous density and temperature of a gas would be accessible using coherent Rayleigh–Brillouin scattering.

The statistical error in the found η_b is determined by the statistical fluctuations in the measured spectra. From the variation in the ten registered spectra, we estimate the rms variation at each (discrete) frequency $\sigma(f_i)$. A slow drift of the laser intensity during the experiment leads to an overestimation of σ. To correct for this, each spectrum was normalized to unity after subtracting the background. The result of this procedure is shown in Fig. 2(a), with the variation σ shown in Fig. 2(c).

A. Extracting the bulk viscosity

In order to extract the bulk viscosity from the spectrum, the measured coherent Rayleigh–Brillouin scattering spectra are compared to the spectra predicted using the Tenti S6 model. In Rayleigh–Brillouin scattering, the dimensionless pressure, or the dimensionless wavelength, is given by the ratio y of the scattering wavelength $2\pi/k$ to the mean free path between collisions

$$y = \frac{p}{kv_0\eta} = \frac{nk_BT}{kv_0\eta}, \tag{1}$$

with k as the scattering wave vector, n as the number density, T as the temperature, p as the pressure, v_0 as the thermal velocity, $v_0 = (2k_BT/M)^{1/2}$, and η as the (shear) viscosity. The Tenti model is based on the Boltzmann equation. The linearized collision integral is approximated with the Wang Chang and Uhlenbeck approach, using six (S6) or seven (S7) moments,[5] of which the S6 model has proven to be superior,[6] possibly due to an effective resummation of the expansion. Although the Tenti models have considerable algebraic complexity, their evaluation only involves the diagonalization of a small matrix and the evaluation of the error function, which can be done extremely quickly on a computer.

From the rms variation at each discrete frequency f_i, $i = 1, \ldots, N$, we determine the normalized difference $\Delta(f_i)$ between model $I_m(f_i)$ and experimental $I_e(f_i)$ spectrum as

$$\Delta(f_i) = \frac{I_m(f_i) - I_e(f_i)}{\sigma(f_i)} \tag{2}$$

and the χ^2 as $\chi^2 = \frac{1}{N}\Sigma_{i=1}^N \Delta^2(f_i)$. The normalized difference is shown in Fig. 2(d). If the computed line shape model I_m would fit the measurement perfectly, then only statistical errors remain and the minimum of χ^2 is unity. Let $\tilde{\eta}_b$ be the value of η_b at which χ^2 has a minimum. Using a maximum likelihood argument, the curvature of the function $\chi^2(\eta_b)$ in this point determines the error in the estimation of the bulk viscosity via

$$\sigma_{\eta_b} = \left(\frac{N'}{2} \frac{d^2\chi^2}{d\eta_b^2} \bigg|_{\tilde{\eta}_b} \right)^{-1/2}, \tag{3}$$

where N' is the number of independent samples in the spectrum. We note that in Eq. (2), the wings of the spectra receive a larger weight than the core region because the wings have smaller fluctuations. However, the estimate for the bulk viscosity is dominated by the core region, as it is affected most by variation of η_b.

The distribution of the noise in the measured spectra and the number N' of independent samples can be estimated from the autocorrelation function $C(f)$ of the normalized difference $\Delta(f_i)$, $C(f) = \langle \Delta(f_i + f)\Delta(f_i) \rangle$, where the average $\langle \ \rangle$ is done over f_i. If the noise is uncorrelated, the correlation function has a peak at $f = 0$ with width equal to the frequency sample distance. This would be the case if the statistical fluctuations correspond to the shot noise in the collected charge of each pixel. The correlation function is shown in Fig. 2(e) and shows this narrow spike in addition to a broad feature related to the fluctuating mode structure. This latter feature shows the correlation between nearby pixels and the number N' of independent spectral samples can be derived from the correlation length. We find $N' \approx 14$ and an estimated error in $\sigma_{\eta_b} = 0.3 \times 10^{-5}$ kg m^{-1} s^{-1} for the gas analyzed in Fig. 2 (O_2 at $p = 5$ bar).

We should realize, however, that σ_{η_b} merely is the statistical error in the measured η_b. An important source of systematic errors is the alignment of the setup, which produces errors comparable to the statistical ones.

The light scattering experiments do not provide an absolute intensity; therefore, both the experimental and computed spectra were normalized such that $\int_{-f_b}^{f_b} I(f)df = 1$, where the integration extends over one FSR, $f_b = \text{FSR}/2$. Since the FSR of the Fizeau spectrometer is always (much) larger than the width of our Doppler-broadened lines, the precise value of f_b is not important.

Another problem is the signal background I_{e_0} in the experiment, which must be subtracted from the raw measured spectrum $I_{e_r}(f)$ before normalization of $I_e(f) = I_{e_r}(f) - I_{e_0}$. The background is mainly made up of the dark current of the (uncooled) CCD array in the Fizeau spectrometer; it is large and of the order of the signal strength. The signal background I_{e_0} was determined by setting the model spectrum $I_m(f) = a(I_e(f) - I_{e_0})$ and determine I_{e_0} and the proportionality constant a in a least-squares procedure for the wings of the spectra. The idea is that it is better to use the wings of a model spectrum rather than fitting a horizontal line to the background. The wings of the spectra were defined as the range of frequencies for which $I_m(f) \leq \max(I_m)/4$. Finally, as the origin of the frequency scale of the Fizeau spectrometer is not determined well, both measured and model spectra were shifted so that their centers lie at $f = 0$. The result of these procedures is shown in Fig. 2(g).

An overview of Rayleigh–Brillouin scattering spectra of polar and nonpolar molecules is shown in Fig. 3. At the relatively large pressures, the Brillouin peaks dominate the spectra and the line shapes depend sensitively on the value of η_b. In a few cases, the mode structure of the pump laser can
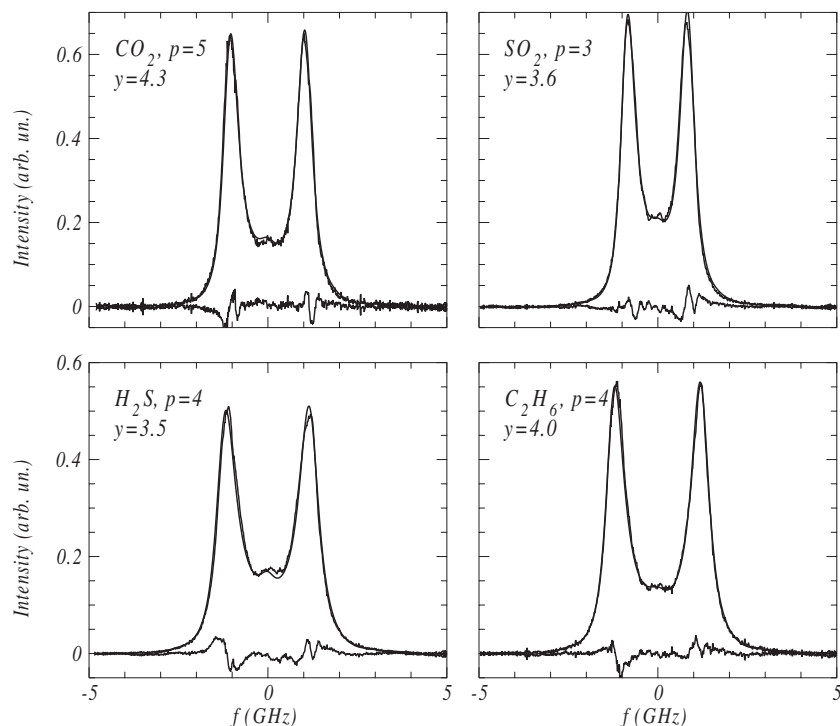
FIG. 3. A few coherent Rayleigh–Brillouin scattering spectra of polar and nonpolar molecules. The measurements are compared to the Tenti S6 model, which was computed using the transport coefficients in Table I.

be recognized in the residues between model and measurement. A summary of the experimental results and a list of the used gas parameters is given in Table I. For the heat capacity of internal degrees of freedom c_{int}, it was assumed that only rotations partake, except in the case of C_2H_6, where torsion also contributes. This will be argued in Sec. III.

The effect of density waves on Rayleigh–Brillouin spectra and the influence of the bulk viscosity is larger when the pressure is higher. Therefore, the results in Table I were obtained at pressures $p=3$ to 5 bar. With the largest reduced pressure $y \approx 4$, the experiments are in the kinetic regime. At lower pressures it was difficult to obtain dependable values of η_b.

Noble gases do not have internal degrees of freedom and do not have a bulk viscosity ($c_{int}=0$, $\eta_b=0$). However, a noble gas cannot be used to check our method because for small c_{int}, the line shape model depends only on η_b/c_{int}^2 and in the limit $c_{int} \to 0$, the line shape becomes independent of η_b.

III. KINETIC MODELS AND BULK VISCOSITY

The shape of molecules affects the transport properties of a gas, both at low and high densities. In this work we investigate the bulk viscosity, which is the transport coefficient most strongly affected by deviations from purely spherical molecules. A comparison among experimental results, results from literature, and theoretical predictions from kinetic models provides insight into the relations among molecular shape, internal degrees of freedom, and transport properties.

From a straightforward extension of the arguments in Ref. 13, the frequency-dependent bulk viscosity can be related to the relaxation time of the internal degrees of freedom

$$\eta_b = 2nk_B T \frac{\Sigma_j N_j \tau_j (1 + i\omega\tau_j)^{-1}}{N(3 + \Sigma_j N_j (1 + i\omega\tau_j)^{-1})}, \qquad (4)$$

where N_j is the number of internal degrees of freedom with relaxation time τ_j, N is the total number of degrees of free-

TABLE I. Experimental results for the bulk viscosity η_b at $T=293$ K, determined at pressure p, along with the dimensionless pressure y, the shear viscosity η, the heat conductivity λ, and the dimensionless heat capacity of internal degrees of freedom $c_{int}=N/2$, where N is the number of internal degrees of freedom.

	p (bar)	y	η_b (10^{-6} kg m^{-1} s^{-1})	η (10^{-6} kg m^{-1} s^{-1})	λ (10^{-2} W K^{-1} m^{-1})	c_{int}
N_2	5	2.9	26 ± 5	17.7	2.52	1
O_2	5	2.7	23 ± 3	20.2	2.58	1
CO_2	5	4.4	5.8 ± 1.0	14.8	1.66	1
SO_2	3	3.6	5.7 ± 1.0	12.7	0.95	3/2
CH_4	4	2.7	24 ± 3	11.1	3.37	3/2
C_2H_6	4	4.0	9.8 ± 0.8	9.4	2.11	5/2
C_2H_4	3	3.3	3.8 ± 0.5	10.3	2.03	3/2
H_2S	4	3.5	15 ± 1	12.2	1.34	3/2

dom, n the molecular number density, and where it is as-
sumed that the internal degrees of freedom do not interact
with other ones having a different relaxation time, and the
density is small. When the frequency ω of sound waves is
much larger than $1/\tau_j$, the mode j remains frozen and does
not contribute to the bulk viscosity. On the other hand, when
ω is much smaller than all relaxation rates, Eq. (4) reduces to
the well-known $\eta_b = 2nk_B T \sum_j N_j \tau_j / N^2$. Gases consisting of
molecules with no coupling between internal degrees of free-
dom and center-of-mass motion, such as noble gases, have
zero bulk viscosity. Vibrational and/or electronic excitations
exist for all atoms and molecules, but at room temperature in
many cases these are not thermally accessible and therefore,
they effectively decouple from the center-of-mass momenta
and the associated relaxation times are extremely long.
Vibration-translation relaxation times for the gases under in-
vestigation here are shown in Table III at a pressure of 1 bar.
In coherent Rayleigh–Brillouin scattering experiments,
where the typical frequency of sound waves is around
1 GHz, the bulk viscosity is thus not affected by vibrational
degrees of freedom with vibration-translation relaxation
times much longer than 1 ns. Therefore, for all gases under
investigation here except ethane, only rotational degrees of
freedom can contribute to the bulk viscosity. In the case of
ethane, one vibrational mode, the torsion mode, has a rela-
tively low-energy excited state, with a relaxation time that is
short enough to contribute. Consequently, at room tempera-
ture, for small molecules at least, interactions due to non-
spherical molecular shape, asymmetry, and dipole moments
dominate the bulk viscosity. In experiments using sound
waves with lower frequencies, however, the vibrational
degrees of freedom are detectable.

In this work we consider four kinetic models with rota-
tional degrees of freedom which interact in a purely classical
way with translation and lead to nonzero bulk viscosity. They
are rigid spherocylinders (SC), loaded rigid spheres (LS),
rigid spheres with embedded point dipoles (ED), and rough
spheres (RS). Each of these models addresses a specific
mechanism for relaxation, and so the success of each model
at describing experimental results for the bulk viscosity gives
an indication as to what kind of interactions dominate the
relaxation of the internal degrees of freedom. Stronger cou-
pling between internal degrees of freedom and the momenta
of two colliding molecules leads to a shorter relaxation time
and thus a smaller bulk viscosity. The models have, at most,
two internal degrees of freedom, both of which have the
same relaxation time.

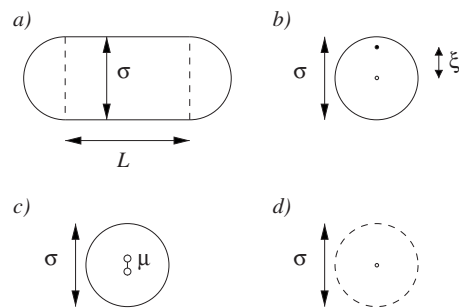Each of the models prescribes how to compute the col-

FIG. 4. Diagrams of the molecules in the various kinetic models. (a) A
spherocylinder, (b) a loaded rigid sphere, (c) a rigid sphere with an embed-
ded point dipole, and (d) a rough sphere. The relevant size parameters are
indicated in each figure.

lision integral and yields a closed expression for the bulk
viscosity. Each of the models, therefore, could be used di-
rectly to compute the line shape of coherent Rayleigh–
Brillouin scattering, following procedures similar to Refs. 8
and 25. However, the key quantity of interest here is the bulk
viscosity and these models might perform poorly in repre-
senting line shapes for which other transport coefficients are
also relevant.

Schematic representations of the four kinetic models are
shown in Fig. 4. Spherocylinders have a length L and diam-
eter σ. All other models consist of rigid spheres with diam-
eter σ, but loaded rigid spheres have a center-of-mass that is
a distance ξ away from the geometrical center, and rigid
spheres with embedded point dipoles have a dipole moment
μ. Rough spheres exchange angular momentum by prescrib-
ing a zero relative surface velocity of colliding molecules.[13]
Each molecule has a mass m and a moment of inertia Γ
around any axis orthogonal to the main symmetry axis in the
case of SC, LS, and ED and around any axis in the case of
RS. The parameters for each model are listed in Table II,
along with the physical properties they model, gases which
have these properties, and references which contain expres-
sions for the bulk and shear viscosities.

Most polyatomic molecules have an elongated shape and
therefore, SC can be used to describe the relaxation of inter-
nal degrees of freedom due to the shape of molecules. Many
polyatomic molecules are asymmetric and their center-of-
mass does not coincide with the geometrical center. This
property is accounted for by the LS model. Asymmetric mol-
ecules typically also have significant dipole moments, the
effects of which are described by the ED model. The RS
model only describes an aspect of molecules consisting of
larger numbers of atoms, such as CH_4 or H_2S, but because of

TABLE II. The four kinetic models considered, the property of gas molecules which they represent, their parameters, which of the gases under investigation
in this work they can be applied to, and references which contain the expressions used for the bulk viscosity and the other transport coefficients. For each
model the spherical radius σ was obtained form the shear viscosity.

Model	Property	Parameters	Gas	References η, η_b
SC	Elongated	L, Γ, m, σ	N_2, O_2, CO_2, SO_2, C_2H_6, C_2H_4, and H_2S	26
LS	Asymmetric center-of-mass position	ξ, Γ, m, σ	H_2S	27
ED	Dipole moment	μ, Γ, m, σ	SO_2 and H_2S	28 and 29
RS	Rough surface	Γ, m, σ	CH_4, C_2H_6, C_2H_4, and H_2S (N_2, O_2, CO_2, and SO_2)	13

TABLE III. The results for η_b from the various models, our experiments, and experimental literature in 10^{-6} kg m^{-1} s^{-1} at T=293 K. The sphere diameter σ is in 10^{-10} m. The literature values of η_b were obtained from experiments at acoustic frequencies, except for CO_2, which was obtained from CRBS. The rotation-translation and vibration-translation relaxation times τ_r and τ_{vib} are shown in nanoseconds at 1 bar and were obtained from Ref. 33, with the exception of the relaxation times of SO_2, which can be found in Ref. 34, and of ethane, which were obtained from Ref. 32. For ethane, the relaxation time of the vibrational mode with the second-fastest relaxation is also indicated. The values of η_b estimated from the relaxation times using Eq. (4). For all gases except ethane, only the rotational relaxation needs to be included. For ethane, the fastest vibrational relaxation time, which is not sufficiently long as to produce negligible effects on the time scales of the coherent Rayleigh–Brillouin scattering experiments, was also included.

	Exp.	SC		LS		ED		RS		Lit.	Lit. relaxation		
	η_b	η_b	σ	η_b	σ	η_b	σ	η_b	σ	η_b	η_b	τ_r	τ_{vib}
N_2	26 ± 5	24	3.20	$\cdots$	$\cdots$	$\cdots$	$\cdots$	34	3.69	12.8[a]	12	0.74	$O(10^8)$
O_2	23 ± 3	28	2.99	$\cdots$	$\cdots$	$\cdots$	$\cdots$	31	3.53	8.2[b]	11	0.69	$O(10^7)$
CO_2	5.8 ± 1.0	18	3.46	$\cdots$	$\cdots$	$\cdots$	$\cdots$	14	4.52	3.7[c]	4.7	0.30	6×10^3
SO_2	5.7 ± 1.0	14	4.40	$\cdots$	$\cdots$	0.13	5.37	18	5.35		1.7	0.10	31
CH_4	24 ± 3	$\cdots$	$\cdots$	$\cdots$	$\cdots$	$\cdots$	$\cdots$	19	4.05	14.5[a]	13	0.76	1.3×10^3
C_2H_6	9.8 ± 0.8	16	4.42	$\cdots$	$\cdots$	$\cdots$	$\cdots$	12	5.15	11.4[d]	7.0	0.25	0.75, 9.5
C_2H_4	3.8 ± 0.5	17	4.20	$\cdots$	$\cdots$	$\cdots$	$\cdots$	15	4.84		2.0	0.12	80
H_2S	15 ± 1	9.1	5.26	31	4.67	0.08	4.67	101	4.67		50	3.0	

[a]Reference 30.
[b]Reference 31.
[c]Reference 9.
[d]Reference 32.

its lack of parameters, can be applied to other gases as well. In those cases it should be seen as a generic model for interaction of rotation.

Not every gas under consideration in this work has all of the properties which the models describe. For instance, the shape of most diatomic gases is roughly spherocylindrical, but if both atoms are the same element, it has no dipole moment and the center-of-mass coincides with the geometric center. For some gases, several models describe different mechanisms for the relaxation of the internal degrees of freedom. In these cases, the kinetic models underestimate the relaxation rate and therefore lead to an overestimation of the bulk viscosity.

The parameters of the kinetic models can be obtained from the bond lengths, bond angles, and the known dipole moments of polar molecules. For polyatomic molecules involving one large atom and several H atoms, the geometrical center was chosen to be at the center of the large atom. In diatomic and triatomic molecules, the length L of a spherocylinder was taken as the distance between the outermost atomic nuclei. For ethane and ethylene, L was taken equal to the CC bond length. In the models, two or three relevant components of the moment of inertia are all equal, but for some of the gas molecules, the relevant components of the moment of inertia are not all the same. In our calculations we use the average of the relevant components. Finally, the diameter σ of the molecules was obtained from the shear viscosity, listed in Table I, using the expressions from the references listed in Table II, and for the ED model the expression for simple rigid spheres.[13] Closed expressions to compute a bulk viscosity from these parameters can be found in the references listed in Table II.[37,38]

From Eq. (4), estimates can also be made of the bulk viscosity from literature values of the rotational relaxation times and, in the case of ethane, from the rotational and vibrational relaxation times. It should be noted, however, that these relaxation times are for the fastest decaying rotational and vibrational degrees of freedom. Molecules such as SO_2, ethylene, and ethane have three rotational degrees of freedom, each with its own moment of inertia, and thus its own distinct relaxation time. Some of these relaxation times may be so long as to not be detectable at the gigahertz frequencies of the coherent Rayleigh–Brillouin scattering experiments. The η_b obtained from Eq. (4), based on a single relaxation time for all rotational degrees of freedom, must therefore be seen as a rough estimate for the bulk viscosity.

IV. DISCUSSION

The experimental results for the bulk viscosity and the results from the four kinetic models are listed in Table III, along with values from experimental literature for bulk viscosity and relaxation times.

In general, we find larger values of the bulk viscosity than those of the literature, including the values computed from the relaxation times. However, the relaxation rates and the bulk viscosities from the literature are often based on similar (acoustic) experiments. An exception is the bulk viscosity of CO_2 measured by Pan et al.[9] who used coherent Rayleigh–Brillouin scattering and rediscovered the observation of Lao et al.[32] that at gigahertz, frequencies the vibration modes remain frozen. Lao et al. found $\eta_b=2.2 \times 10^{-6}$ kg m^{-1} s^{-1}. The estimates of the bulk viscosity of H_2S from the relaxation times are not reliable because the rotational relaxation time is relatively long. For this case, the frequency dependence in Eq. (4) predicts a reduction of the zero-frequency η_b of $(1+(\omega\tau_r/2)^2)^{1/2} \approx 9.5$. Interestingly, Eq. (4) predicts a pressure-dependent bulk viscosity at pressures around 10 bar.

One can see from Table III that the spherocylinder and rough-sphere models predict the correct order of magnitude

for all molecules. The loaded spheres model is not applicable to many molecules, as it is not always possible to determine an eccentricity.

Intuitively, one expects polar molecules to have a very low bulk viscosity because the embedded dipole facilitates the coupling of angular momentum to linear momentum in collisions. Indeed, this is also predicted by the ED model. Surprisingly, the experimental value of η_b for H_2S is more than two orders of magnitude larger than the prediction of the ED model.

For the most ideal spherocylinder molecules, N_2 and O_2, the agreement between model and experiment is good. For N_2, O_2, CH_4, and C_2H_6 the rough-sphere model predicts bulk viscosities in fair agreement with experiments; on other molecules it predicts the right order of magnitude. This is remarkable because the only parameter of the RS model is the sphere radius, and unlike in the other models, there is no additional parameter to describe the angular momentum exchange.

Several of the gases under consideration here have properties which are not modeled correctly by any of the four kinetic models. As can be seen from the rotation-translation relaxation times in Table III, for ethane, the relaxation of vibrational modes contributes to the bulk viscosity as well. Additionally, the rotational quantum states of H_2S are not so close together and it may be necessary to describe the molecules quantum-mechanically to obtain reliable results. It should be noted in this context that Olmsted *et al.*[28] also obtained quantum-mechanical results from a distorted wave approximation.

V. CONCLUSION

We have exploited coherent Rayleigh–Brillouin scattering as an efficient machinery to learn about bulk viscosities at the gigahertz frequencies which are relevant for light scattering. As the statistical error in the η_b results owes to the fluctuating mode structure of the pump laser, much can be gained in this technique by using a pump laser with a smooth broadband spectral profile.

Our spectra could be described adequately by the Tenti S6 model;[6] elsewhere we show that the earlier Tenti S7 model[5] differs significantly from the measured lineshapes.[35] Clearly, the statistics must be improved in order to further test the adequacy of line shape models, and the wavelength (y-parameter) dependence of η_b.

The bulk viscosity is a subtle transport coefficient which depends both on rotational and vibrational degrees of freedom.[36] Because the relaxation of vibrational energy is slow, those degrees of freedom remain frozen at the gigahertz sound frequencies of this experiment for most small molecules and bulk viscosity is due to the effect of rotations alone. Thus, coherent Rayleigh–Brillouin scattering offers a more simple testing ground for kinetic models than acoustic experiments where vibrations do play a role. Remarkably, the simple kinetic models considered in this paper predict the value of η_b to within a factor of 2. Molecules with a permanent dipole moment, however, have a surprisingly large η_b, while much lower values were expected.

[1] ADM-Aeolus, April 2008 (European Space Agency, 2008).
[2] V. Ghaem-Maghami and A. D. May, Phys. Rev. A **22**, 692 (1980).
[3] A. T. Young and G. W. Kattawar, Appl. Opt. **22**, 3668 (1983).
[4] R. B. Miles, W. N. Lempert, and J. Forkney, Meas. Sci. Technol. **12**, R33 (2001).
[5] C. D. Boley, R. C. Desai, and G. Tenti, Can. J. Phys. **50**, 2158 (1972).
[6] G. Tenti, C. D. Boley, and R. C. Desai, Can. J. Phys. **52**, 285 (1974).
[7] X. Pan, M. N. Shneider, and R. B. Miles, Phys. Rev. Lett. **89**, 183001 (2002).
[8] X. Pan, M. N. Shneider, and R. B. Miles, Phys. Rev. A **69**, 033814 (2004).
[9] X. Pan, M. N. Shneider, and R. B. Miles, Phys. Rev. A **71**, 045801 (2005).
[10] J. Xu, X. Ren, W. Gong, R. Dai, and D. Liu, Appl. Opt. **42**, 6704 (2003).
[11] X. Pan, M. N. Shneider, Z. Zhang, and R. B. Miles, "The 42nd Aerospace Sciences Meeting and Exhibit Conference," AIAA Paper No. 2004-0017, 2004, Vol. 1.
[12] K. F. Herzfeld and T. A. Litovitz, *Absorption and Dispersion of Ultrasonic Waves* (Academic, London, 1959).
[13] A. Chapman and T. G. Cowling, *Mathematical Theory of Non-Uniform Gases*, 3rd ed. (Cambridge Mathematical Library, Cambridge, UK, 1970).
[14] D. D. Royal, V. Vesovic, J. M. Trusler, and W. A. Wakeham, Mol. Phys. **101**, 339 (2003).
[15] A. de Wijn, N. Riesco, V. Vesovic, G. Jackson, and J. M. Trusler (to be published).
[16] A. S. de Wijn, V. Vesovic, G. Jackson, and J. P. Trusler, J. Chem. Phys. **128**, 204901 (2008).
[17] J. H. Grinstead and P. F. Barker, Phys. Rev. Lett. **85**, 1222 (2000).
[18] M. N. Shneider, P. Barker, X. Pan, and R. Miles, Opt. Commun. **239**, 205 (2004).
[19] H. Bookey, A. Bishop, M. N. Shneider, and P. Barker, J. Raman Spectrosc. **37**, 655 (2006).
[20] H. Bookey, M. N. Shneider, and P. Barker, Phys. Rev. Lett. **99**, 133001 (2007).
[21] L. Westling, M. Raymer, and J. Snyder, J. Opt. Soc. Am. B **1**, 150 (1984).
[22] P. Langenbeck, Appl. Opt. **9**, 2053 (1970).
[23] J. R. Rogers, J. Opt. Soc. Am. **72**, 638 (1982).
[24] T. T. Kajava, H. M. Lauranto, and A. T. Friberg, J. Opt. Soc. Am. A **11**, 2045 (1994).
[25] W. Marquez, Jr., J. Stat. Mech.: Theory Exp. 2007, P03013.
[26] C. Curtiss and C. Muckenfuss, J. Chem. Phys. **26**, 1619 (1957).
[27] S. Sandler and J. Dahler, J. Chem. Phys. **43**, 1750 (1965).
[28] R. Olmsted and C. Curtiss, J. Chem. Phys. **55**, 3276 (1971).
[29] L. Monchick and E. Mason, J. Chem. Phys. **35**, 1676 (1961).
[30] G. Prangsma, A. Alberga, and J. Beenakker, Physica (Amsterdam) **64**, 278 (1973).
[31] P. Thompson, *Compressible-Fluid Dynamics* (McGraw-Hill, New York, 1972).
[32] Q. H. Lao, P. E. Schoen, and B. Chu, J. Chem. Phys. **64**, 3547 (1976).
[33] J. Lambert, *Vibrational and Rotational Relaxation in Gases* (Clarendon, Oxford, 1977).
[34] H. Bass, T. Winter, and L. Evans, J. Chem. Phys. **54**, 644 (1971).
[35] M. O. Vieitez, E.-J. van Duijn, W. Ubachs, A. Meijer, A. S. de Wijn, N. J. Dam, B. Witschas, and W. van de Water, Phys. Rev. A **82**, 043836 (2010).
[36] W. E. Meador, G. A. Milner, and L. W. Townsend, Phys. Fluids **8**, 258 (1996).
[37] The expression for the viscosity of ED can be obtained from the result of Monchick *et al.* (Ref. 29) for polar molecules with a general, otherwise

spherical, interaction potential in terms of collision integrals. However, in their calculations of the viscosity, Monchick *et al.* made the assumption that the trajectories and orientations of two colliding molecules are not altered significantly by the dipole moment. This approximation of weak dipole-dipole interaction is not valid for SO_2 and H_2S, but the viscosity is not strongly affected by the dipole-dipole interaction. Therefore, the diameters of these molecules were estimated from the shear viscosity by using the expression for simple rigid spheres (Ref. 13). Because of the weak dipole approximation, Monchick *et al.* could also not calculate a bulk viscosity. Olmsted *et al.* (Ref. 28) later succeeded in calculating the relaxation time of the rotational degrees of freedom, which can be used to obtain the bulk viscosity from Eq. (4).

[38] Note that Sandler *et al.* (Ref. 27) obtained their expressions for loaded spheres through an expansion in the eccentricity, which are therefore only valid if the center-of-mass is relatively close to the geometrical center, which is the case for H_2S.